Ricardo Figueiredo Rosa

# Microfluidic Fabrication of Porous Silicon Based Acid-Degradable Nanocomposites for Drug Delivery Applications

Monografia realizada no âmbito da unidade Estágio Curricular do Mestrado Integrado em Ciências Farmacêuticas, orientada pelo Professor Doutor António José Ribeiro e apresentada à Faculdade de Farmácia da Universidade de Coimbra

Setembro 2014

· U C ·

UNIVERSIDADE DE COIMBRA

Eu, Ricardo Figueiredo Rosa, estudante do Mestrado Integrado em Ciências Farmacêuticas, com o nº 2009010688, declaro assumir toda a responsabilidade pelo conteúdo da Monografia apresentada à Faculdade de Farmácia da Universidade de Coimbra, no âmbito da unidade Estágio Curricular. Mais declaro que este é um trabalho original e que toda e qualquer afirmação ou expressão, por mim utilizada, está referenciada na Bibliografia desta Monografia, segundo os critérios bibliográficos legalmente estabelecidos, salvaguardando sempre os Direitos de Autor, à exceção das minhas opiniões pessoais.

O estudante,

_____

(Ricardo Figueiredo Rosa)

Coimbra, _____ de _____de 2014.

O estudante,

_____

(Ricardo Figueiredo Rosa)

O tutor da faculdade,

_____

(Professor Doutor António José Ribeiro)

Coimbra, _____ de _____de 2014.

## Acknowledgements

The studies that resulted in this monograph were conducted in the Pharmaceutical Nanotechnology & Chemical Microsystems (NAMI) unit of the Faculty of Pharmacy of the University of Helsinki, between the 22nd of January and the 20th of April of 2014. This opportunity was provided by the Erasmus program, but it wouldn't have been possible without the relentless help and guidance of Dr. Hélder Santos, Dr. Donfgei Liu, and Dr. António Ribeiro, in the condition of home university supervisor. I would like to express my endless gratitude to all of these excellent teachers, as well as to all NAMI unit, who has welcomed me during my time in Finland in the most familiar and warmful manner.

On a different note, my feelings of appreciation and respect towards the Faculty of Pharmacy of the University of Coimbra and its docents will endure and accompany me as I now start a new chapter of my life.

To my family and loved ones, I feel truly blessed to have shared this journey with you and I can't wait to perceive what the future will bring in our way.

## Abstract

Combination therapy represents the most promising strategy for the treatment of cancer. The co-loading of different therapeutic molecules within the same carrier enables the delivery of a desirable ratio of each drug to the target of interest, accomplishing synergistic therapeutic effects between the drugs, while suppressing drug resistance.

The aim of this study was to use a one-step microfluidic nanoprecipitation method to produce porous silicon (PSi)/acid–degradable polymer nanocomposites with precise and ratriometric loading of the breast cancer drugs methotrexate (MTX), sorafenib (SFN) and paclitaxel (PTX), for their posterior pH-controlled release in the intracellular environment.

The loading of the different drugs was achieved by firstly loading the MTX within the amine–terminated thermally carbonized-PSi (TCPSi) nanoparticles, which were then dispersed into an acetalated-dextran (AcDX) matrix containing PTX and SFN. The microfluidic technique was then used to encapsulate the drug loaded TCPSi nanoparticles within the AcDX, through nanoprecipitation (PSi@AcDX). Finally, the PSi@AcDX nanocomposites were functionalized with a cell penetrating peptide (CPP), to enhance the cellular uptake of the obtained nancomposites.

The physicochemical analysis of the synthesized particles, including PSi, PSi@AcDX and CPP-functionalized PSi@AcDX (PSi@AcDX-CPP), confirmed the successful assembly of the nanocomposites, resulting in improved surface smoothness and homogenous size distribution. The fabricated PSi@AcDX-CPP exhibited high level of cell uptake, high cytocompatibility and, due to their tunable multi-drug payloads, a significant impact on MCF-7, and MDA-MB-231 proliferation profiles, granting this system as an attractive multidrug delivery platform.


**Key words:** Microfluidics, porous silicon, nanoparticles, acid-degradable, combination therapy.

## Resumo

A associação terapêutica de fármacos antineoplásicos e sua consequente formulação num mesmo sistema de administração potencia o seu efeito sinergético na terapia do cancro, ao mesmo tempo que contribui para a diminuição da resistência das células cancerígenas aos mesmos.

Nesse sentido, o objectivo do presente estudo é tirar proveito de uma tecnologia de microfluído para fabricar nano-transportadores, híbridos constituídos por nano-partículas porosas de silício e por um polímero de dextrano modificado que permitam a encapsulação, no seu interior, de três fármacos utilizados no tratamento do cancro da mama (metotrexato, sorafenib e placitaxel) e a sua posterior libertação no meio intracelular, motivada pelo decréscimo do valor de pH.

Primeiramente, o metotrexato foi encapsulado dentro das nano-partículas de silício, que foram então dispersas numa solução de polímero contendo sorafenib e paclitaxel de onde, através de processos de nanoprecipitação potenciada por convergência de fluídos, foram obtidos os nano-transportadores. Por fim, as partículas recém-formadas foram funcionalizadas com um peptídeo, com o objectivo de aumentar a sua internalização pelas células.

Uma posterior análise físico-química corroborou a formação das nano-partículas pretendidas, a uniformidade da sua superfície e homogeneidade de tamanho. Após todo o processo de experimentação, as nano-partículas sintetizadas exibiram elevada capacidade de serem internalizadas pelas células, elevada citocompatibilidade e, devido ao seu cuidadosamente regulado conteúdo terapêutico, um impacto significativo no perfil de proliferação de linhas celulares do cancro da mama.


**Palavras-chave:** Tecnologia de microfluído, nano-partículas porosas de silício, valor de pH, associação terapêutica.

# Table of contents

## Abbreviations

AcDX – Acetalated dextran

APTES – (3-aminopropyl)triethoxysilane

ATR – Attenuated total reflectance

CPP – Cell penetrating peptide

DDS – Drug delivery systems

DLS – Dynamic light scattering

DMEM – Dulbecco's modified eagle medium

DMSO – Dimethyl sulfoxide

FITC – Fluorescein isothiocyanate

FTIR – Fourier transformed infrared spectroscopy

HBSS – Hank's balanced salt solution

HF – Hydrofluoric acid

MTX – Methotrexate

MTX-PSi – Methotrexate loaded porous silicon

MW – Molecular weight

NPSi – Nanostructured porous silicon

P-188 – Poloxamer 188

PBS – Phosphate buffer solution

PTX – Paclitaxel

PSi – Porous silicon

PSi@AcDX – Porous silicon encapsulated within acetalated dextran

PSi@AcDX-CPP – Porous silicon encapsulated within acetalated dextran and functionalized with the cell penetrating peptide

PSi-FITC – Fluorescein isothiocyanate labelled porous silicon

PVA – Polyvinyl alcohol

RPM – Revolutions per minute

RPMI 1640 – Roswell park memorial institute 1640

SFN – Sorafenib

TEA – Triethylamine

TEM – Transmission electron microscopy

TCPSi – Thermally carbonized porous silicon

THCPSi – Thermally hidrocarbonized porous silicon

TOPSi – Thermally oxidized porous silicon

## 1. Introduction

Nanotechnology is one of the fastest growing areas of the pharmaceutical sector, a research field that is potentiating not only the evolution, but also the revolution of science and the entrance on a new pharmaceutical paradigm. The ability to engineer and manufacture materials at nanoscale represents a tremendous progress for pharmaceutical industries and stands as a promising tool to enhance drug delivery and enable new diagnosis and therapeutic approaches for both well-known and emerging diseases, such as diabetes, cardiovascular diseases and cancer.[1-5]

According to Lux Research, by 2015, the worldwide value spent on nanotechnology will raise to $2.6 trillion.[6] Considering the advanced drug delivery systems (DDS) alone, the amount invested in 2008 was up to $134.3 billion and is estimated to increase to $196.4 billion in 2014.[7]

Ever since its discovery, the nanoscale DDS, including nanovectors, have been proving to perform an important role in successfully maximizing the therapeutic efficacy of drugs, while reducing their associated side effects.[2] Nowadays, the most frequently discussed nanovectors are polymer-based platforms, dendrimers, gold nano-shells, semiconductor nano-crystals, biologically derived nano-constructs, and mesoporous silicon- and silica-based nanosystems.[2]

It has been shown that unfavorable physicochemical properties of many drug molecules affect their formulation into therapeutic vehicles, bioavailability and, consequently, the efficacy of the treatment.[7, 8] Moreover, besides these drugs' physicochemical properties, the optimization of other crucial technological parameters such as shape, size, surface properties, porosity, and compartmentalization of the carriers [8] has evoked further investigation regarding the development of more advanced DDS and therapies.

Due to these increasingly sophisticated therapy strategies, coadministration of multiple drugs is often desired, but extremely complex to achieve. The co-loading of different drugs within the same nanocarrier system privileges their synergistic therapeutic effect, enables the delivery of a correct ratio of each drug to the target of interest while suppressing drug resistance and controlling drug exposure over time.[9-12]

Even though traditional drug loading of nanocarriers has been accomplished for hydrophobic cargos, the concurrently deliver of both hydrophobic and hydrophilic payloads may represent the most promising and relevant accomplishment for the future of multidrug-therapy, but has yet remained challenging to achieve without chemical drug conjugations.[13,

[14] Consequentially, there is the need to explore the potentialities of new techniques and materials, such as the above mentioned mesoporous silicon- and silica-based nanosystems.

Nanostructured porous silicon (NPSi) has emerged as a promising, biocompatible and biodegradable material (PSi degrades to nontoxic silicic acid *in vivo*, being excreted into urine as orthosilicic acid)[15-17] with a wide range of biomedical applications.[8] NPSi is a well-characterized, versatile, inorganic material[18] obtained by electrochemical anodization of silicon (Si) in hydrofluoric acid (HF) based solutions, whose properties depend on various etching parameters.[8]

Ever since Leigh Canham firstly reported the biocompatibility of NPSi in 1995,[19] it was acknowledged that NPSi's large surface area (>700 $m^2/g$) and great pore volume (> 0.9 $cm^3/g$) enable this material to be used as reservoirs for storing drug molecules, while acting as a protective agent against mechanical stress, pH, and fast degradation. In addition, the possibility of fine tuning the size, and porous structure of PSi has rendered this material versatile as drug delivery carriers.[8].

However, it has been shown that NPSi as such, without any chemical surface modification, is not stable even at room temperature,[20] which led to the development of stabilizing surface treatments,[18, 21] such as thermal hydrocarbonization (THCPSi), thermal oxidation (TOPSi), and thermal carbonization (TCPSi).[8]

Differences in the stabilization methods of the particle surface play a key role on the type of drugs that can be loaded within the porous network, as well as on the process and efficiency of drug loading and release.[22, 23] In the end, this relatively inexpensive, chemically inert, and thermally stable porous "honeycomb" structured PSi material may provide the answer, not only for optimizing drug loading and release, but also for overcoming formulation problems, storing from small hydrophobic/hydrophilic molecules and peptides to more complex chemical entities. [8, 12, 13]

Due to the freely accessible pores of bare NPSi, the drugs that have been initially loaded within these pores can be displaced, as the particles contact with certain constituents in the body fluids, resulting in premature drug release and/or decomposition.[16] To overcome this drawback, it is necessary to protect the pores of the NPSi particles. One of the most efficient ways to shield the loaded PSi is through their encapsulation, accomplished by a bottom-up assembly approach based on nanoprecipitation.[24, 25]

However, in bulk, this method lacks precise control over the mixing processes, resulting in poor reproducibility, polydisperse size distribution and variations in the

nanoparticles' physicochemical properties.[19, 20]Therefore, new technological approaches, such as microfluidics, are needed to overcome these issues.[26]

Microfluidic systems can be described as the technology of manipulating nanolitre volumes in microscale fluidic channels,[27] and are being proved useful both for analytical purposes (e.g., for culturing and analyzing cells for diverse pharmaceutical studies) and as engineering tools (e.g., for synthesizing nanoscale biomaterials, i.e. diagnostic oriented particles and therapeutics drugs).[28]

Microfluidics' interest for the present study lies in the latter application where, by allowing the control and manipulation of the flow rates of the involved fluids [29], this technique regulates the nano- and microscale interactions among precursors, assuring effective control over the physicochemical characteristics of the produced nanocarriers [29]. This way, the application of microfluidic dynamics leads to narrow sized distributed, highly batch-to-batch reproducible, inexpensive and high-throughput production of multi-layer DDS.[27, 30]

The composites formed by using the microfluidic method for embedding the PSi particles within solid carrier matrices combine the advantages of every intervenient, rendering this procedure the ability to greatly enhance the production of multi-drug loaded NPSi with the goal of delivering the therapeutics in a spatiotemporal controlled manner: [16, 17, 22] at the desired sites, with the required rate, and for a suitable time period, with minimized cytotoxicity,[31] as it will be further explained.

The aim of the present study was to fabricate pH-responsive PSi/polymer hybrid nanoparticles, with precise and ratiometric controlled drug loading and release of three breast cancer drugs: methotrexate (MTX), paclitaxel (PTX) and sorafenib (SFN) in the intracellular environment.

For producing this advanced DDS, a microfluidic co-flow technology was employed.[32] The DDS comprised (3-aminopropyl)triethoxysilane (APTES)–TCPSi functionalized particles[33] - TCPSi are extremely stable, presenting hydrophilic surface nature and negative surface charge - which were encapsulated within a pH-responsive biocompatible polymer, acetalated dextran (AcDX),[34] with the purpose of temporarily seal the pores of the PSi nanoparticles. The AcDX polymer, due to its termini, is fundamental for the last step of the process, allowing the ultimate functionalization of the nanoparticles.[35, 36]

The water insoluble PSi/AcDX mixture present in the inner fluid (ethanol) self-assembled into polymer hybrids as it was focused by the outer continuous fluid (aqueous solution containing polyvinyl alcohol – PVA), synthesizing PSi@AcDX nanocarriers.

In the attempt of increasing the cell uptake of the carrier, the PSi@AcDX termini were functionalized with aminooxyacetyl-K-$(R)_9$-COOH, a cell penetrating peptide (CPP),[37]through oxime click chemistry – PSi@AcDX-CPP.[38] The process and the aim of the following experiments can be disclosed in **Figure 1.**

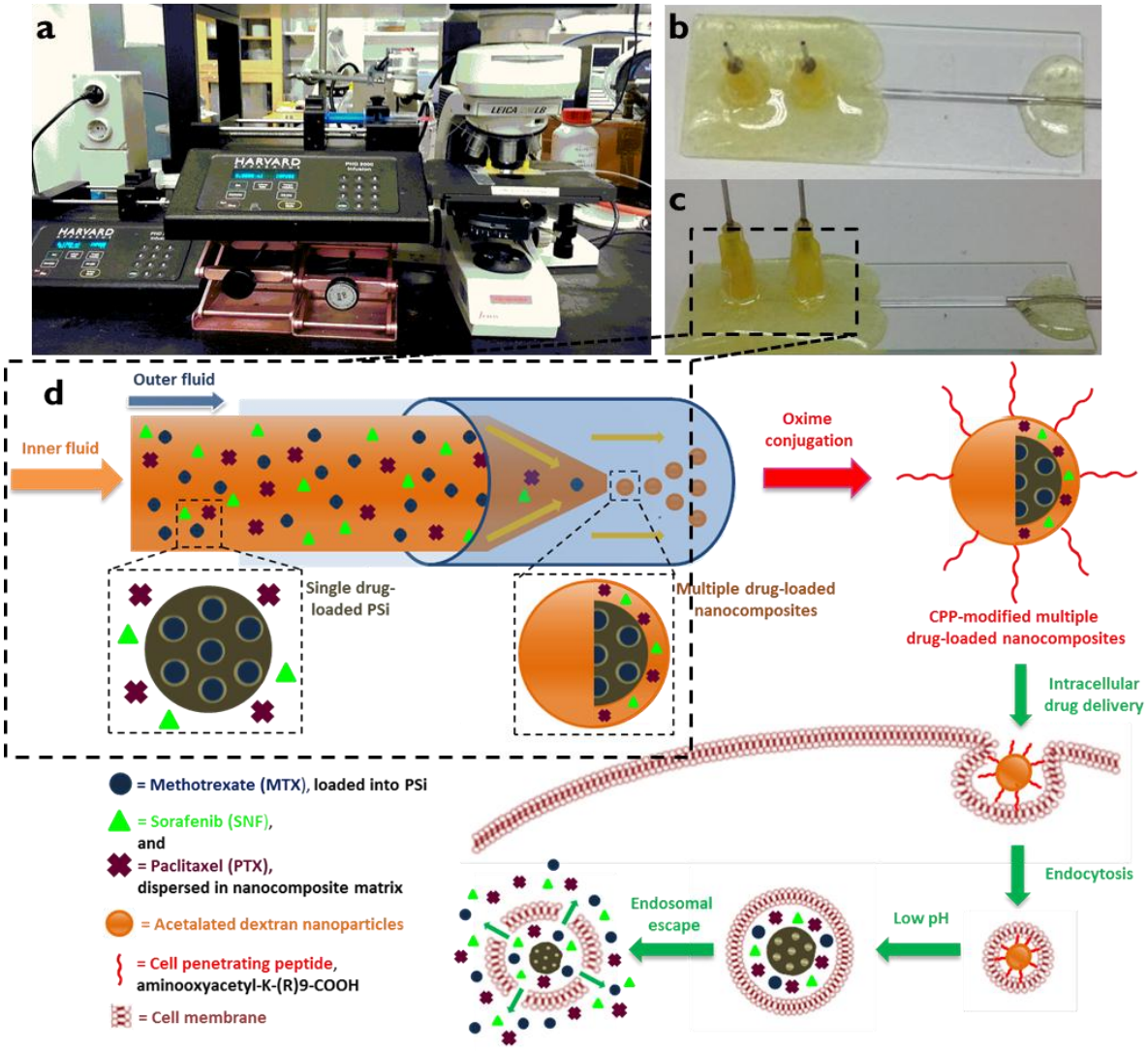


**Figure 1.** *Microfluidic device set-up (a) and overall view of the co-flow microfluidic chip (b-c). Schematic illustration (d) of the process used to synthesize CPP-modified multi-drug loaded pH-responsive polymer/PSi nanocomposites (PSi@AcDX-CPP) and the successive steps of internalization of functionalized particles, followed by endosomal escape and drug release (not to scale). The preparation of PSi@AcDX-CPP is accomplished by co-flow nanoprecipitation method by microfluidics, after which the CPP is attached to the surface of the newly assembled particles by oxime click chemistry. With the help of CPP, the multi-drug loaded PSi@AcDX can travel through distinct intracellular trafficking pathways.*

## 2. Materials and Methods

### 2.1. Fabrication and functionalization of the PSi nanoparticles

Multilayer PSi films were produced by the electrochemically etching of monocrystalline p+-type Si ⟨100⟩ wafers, in a 1:1 (v/v) aqueous HF (38%)–ethanol electrolyte, as described elsewhere.[33] The resulting free films were thermally carbonized with acetylene to obtain TCPSi, which were then treated with HF to generate silanol termination for the APTES functionalization, following the previously described process.[33]

### 2.2. Synthesis of acetalated–dextran

A flame-dried flask was charged with dextran (MW = 10500 g/mol, 1.00 g, 0.095 mmol) and purged with dry $N_2$. Anhydrous dimethyl sulfoxide (DMSO; 10 mL) was added and the resulting mixture was stirred until complete dissolution of the dextran was observed.[34] After adding pyridinium p-toluenesulfonate (15.6 mg, 0.062 mmol) and 2-methoxypropene (3.4 mL, 37 mmol), the flask was placed under a positive pressure of $N_2$, then sealed to prevent evaporation of 2-methoxypropene.[34]

After 3h, the reaction was quenched with triethylamine (TEA, 1mL, 7 mmol), leading to the precipitation of the modified dextran into deionized $H_2O$ (100 mL). The product was isolated by centrifugation and then washed twice with Mili-Q $H_2O$ by vortexing and sonication followed by centrifugation and removal of the supernatant.[34]

Residual water was removed by vacuum oven drying, yielding the acetalated–dextran (AcDX) as a fine white powder.

### 2.3. Fabrication of a glass-capillary microfluidic co-flow device

The microfluidic co-flow chip was contrived by assembling borosilicate glass capillaries on a glass slide.[39] One end of the cylindrical capillary (World Precision Instruments, Inc.), consisting of an inner and outer diameters of around 580 and 1000 μm, respectively, was tapered to a diameter of 20 μm, using a micropipette puller (P-97, Sutter Instrument Co., USA); this diameter was further enlarged to *ca.* 40 μm using a microforge (P-97, Sutter Instrument Co., USA). This cylindrical tapered capillary was inserted into the left end of the square capillary with inner dimension of around 1000 μm (Vitrocom, USA), and coaxially aligned. A transparent epoxy resin (5 Minute® Epoxi, Devcon, USA) was used to seal the capillaries. Two miscible liquids were injected separately into the microfluidic device through polyethylene tubes attached to syringes at constant flow rates. The flow rate of the different liquids was controlled by pumps (PHD 2000, Harvard Apparatus, USA).

### 2.4. Preparation of the pH-responsive nanocomposites

In this process, bare PSi particles were suspended into AcDX in ethanol (10 mg/mL), serving as the inner dispersed phase; while polyvinyl alcohol (PVA, 31–50 kD, 1 mg/mL) aqueous solution was selected as the outer continuous fluid. The inner (3 mL/h) and outer (100 mL/h) fluids were separately pumped into the microfluidic device, in which the inner fluid was focused by the outer continuous fluid. The water insoluble PSi/AcDX self-assembled into polymer hybrids during precipitation from ethanol solutions into water, originating PSi@AcDX nanocarriers.

For the preparation of the bare AcDX particles, the procedure was exactly the same as described for PSi@AcDX, except for the absence of PSi dispersed in the inner fluid.

### 2.5. Functionalization of nanocomposites with CPP

PSi@AcDX was suspended in phosphate buffer solution (PBS) at a certain concentration. The samples were centrifuged and the supernatant removed. The particles were then resuspended by sonication in solutions of aminooxyacetyl-K-$(R)_9$-COOH (10 mg/mL in PBS, pH 7.4), where they were gently agitated for 48h, before being washed with 1×Hank's balanced salt solution (1×HBSS, pH 7.4). The same procedure was adopted for preparing drug-loaded nanovectors functionalized with CPP.

### 2.6. Characterization of the pH-responsive nanocomposites

Particle size was determined using dynamic light scattering with a Zetasizer NanoZS (Malvern Instruments Ltd., UK). For each measurement, the sample (1.0 mL) was loaded in a disposable polystyrene cuvette (SARSTEDT AG & Co., Germany). The nanocarriers' surface $\zeta$-potential was measured with Zetasizer NanoZS by using disposable folded capillary cells (DTS1070, Malvern, UK). Both the $\zeta$-potential and the particle size were recorded as the average of three measurements.

The chemical composition and interaction with the PSi surface, AcDX and CPP, were characterized by Fourier transformed infrared spectroscopy (FTIR) instrument (Vertex 70, Bruker, USA), via horizontal Attenuated Total Reflectance (ATR) accessory (MIRacle, PIKE Technologies, USA). The FTIR spectra were recorded at room temperature between 4000-650 $cm^{-1}$ with a resolution of 4 $cm^{-1}$ using an OPUS 5.5 software.

The structure of fabricated nanocarriers was evaluated by transmission electron microscopy (TEM; Tecnai, FEI Company, USA) at an acceleration voltage of 120 kV. The TEM samples were prepared by depositing 2 µL of the nanocarrier suspension (20 µg/mL for

PSi; 1 mg/mL for the other nanocarriers) onto carbon-coated copper grids (300 mesh; Electron Microscopy Sciences, USA). Excess of solvent was removed from the sample after 5 min incubation, and grids were negatively stained for 5 min at room temperature with sterile-filtered uranyl acetate aqueous solution (2%, w/v). The grids were then washed twice with distilled water and air-dried prior to imaging.

For investigating their dissolution behavior under different pH conditions, the PSi nanoparticles, AcDX nanoparticles and CPP-functionalized nanocomposites were added into the buffer solution (pH 7.4 and 5.0) with the concentration of 1 mg/mL. At different time-points, samples (200 µL) were withdrawn and immediately treated with TEA solution (0.01%, v/v; 1 mL, pH 8) to stop the degradation of AcDX. Afterwards, samples were centrifuged (5 min, 10000 rpm), and then redispersed in the TEA solution by ultrasonication (10 s, 30% amplitude). Finally, the samples underwent TEM imaging, using the same procedure as previously described.

### 2.7. Drug loading and drug encapsulation efficiency of the nanocomposites

MTX was loaded into PSi using an immersion method,[40, 41] by which the particles were added into the MTX solution (40 mg/mL, pH 8.0) with the weight ratio of 1:10 (PSi:MTX), followed by 2 h stirring at room temperature. Afterwards, the suspension was centrifuged (16100 *g*, 3 min; 5415D, Eppendorf, Germany) to remove the excess free drugs, obtaining precipitated MTX-loaded PSi (MTX–PSi). For the preparation of multi-drug loaded nanocomposites, MTX–PSi was dispersed into a free MTX saturated AcDX inner fluid, with posterior addition of the relatively high soluble PTX and SFN. The final steps of the particles preparation procedure continued as described before.

For assessing the loading degree of the nanocomposites, expressed as [(weight of loaded drug/weight of drug loaded samples) × 100%], the particles were immersed into ethanol to dissolve the polymer and release all the payloads. The encapsulation efficiency was defined as the ratio of the actual and the original amounts of drug encapsulated in the carriers, expressed as [(the actual amount of loaded drug/theoretical amount of loaded drug) × 100%].

The amounts of MTX, PTX, and SFN were quantified by HPLC using an Agilent 1100 (Agilent Technologies, USA). PTX and SFN were simultaneously determined with a mobile phase composed of water and acetonitrile (35:65, v/v), while for MTX, a mixture of pH 6.0 buffer solution (0.2 M dibasic sodium phosphate and 0.1 M citric acid) and acetonitrile (ratio of 90:10, v/v) was used. The wavelengths used for quantification of MTX, PTX, and SFN were, respectively, 302, 227 and 265 nm. For all three drugs, a Discovery® C18 column (4.6

× 150 mm, 5 µm, Supelco Analytical, USA) was used as stationary phase, being the flow rate of mobile phase set at 1.0 mL/min, the temperature at 30 °C, and the sample injection volume at 20 µL.

### 2.8. *In vitro* drug release tests

To simulate the extracellular (pH ~7.4) and intracellular (endosome, pH ~5.0) environment, buffer solutions with pH-values of 7.4 and 5.0, and gradient pH media ranging from 7.4 to 5.0, were used in this study. In order to evaluate the *in vitro* release of MTX, PTX, and SFN, drug loaded nanocomposites (*ca.* 1500 µg) were put into the buffer solutions and shook uninterruptedly at 100 rpm and 37 ± 1 °C. Free MTX, PTX, and SFN served as control. In order to optimize drug solubility, amphiphilic Poloxamer 188 (P-188, 5%, w/v) was added into all release media. At previously established time-points, samples of 200 µL were withdrawn and the same volume of preheated medium was added back to replace the withdrawn volume. Finally, samples were sequentially centrifuged (16100 *g*, 3 min) and its concentration quantified by HPLC, as described before.

### 2.9. Cellular uptake analysis of the fabricated particles

For assessing the cellular association of the particles, flow cytometry analysis was conducted. Firstly, the PSi nanoparticles were covalently labeled with fluorescein isothiocyanate isomer I (FITC). In summary, PSi nanoparticles (2mg) were mixed with FITC-ethanol solution (200 µg/mL, pH 7.8) for 2h. The FITC labelled PSi (PSi-FITC) was isolated from the reaction mixture and washed three times with ethanol to remove the unreacted FITC. Afterwards, the FITC labelled PSi@AcDX was prepared by encapsulating the PSi-FITC nanoparticles within AcDX.

At first, MCF-7, and MDA-MB-231 cancer cells (American Type Culture Collection, USA), were seeded and incubated in a 6-well plate ($2\times10^5$ cells/mL, 2.5 mL/well). Following 24 h attachment to the walls, at 37 °C, the cell medium was removed, and the wells were washed twice with 1×HBSS (pH 7.4). Afterwards, 2.5 mL of each sample (100 µg/mL) were incubated with the cells for 6h.

After the incubation period and posterior washing, cells were harvested and treated with trypan blue (0.04% v/v; MP Biomedicals, LLC, Germany) to quench the fluorescence of possible surface adherent particles, thus discriminating the cell-particle association and particle internalization.

Flow cytometry was then performed with an LSR II flow cytometer (BD Biosciences, USA) with laser excitation wavelength of 488 nm using a FACSDiva software. About 10 000

events were obtained for each sample. Data were analyzed and plotted using Flowjo software (Tree Star Inc., USA).

### 2.10. Cytocompatibility of the pH-responsive nanocomposites

Breast cancer cells, MCF-7 and MDA-MB-231 were used for testing the cytocompatibility of the bare nanocarriers. MCF-7 cell Dulbecco's Modified Eagle Medium (DMEM) suspension and MDA-MB-231 cell Roswell Park Memorial Institute 1640 (RPMI 1640) suspension were both seeded into 96-well plates ($2.0\times10^5$ cells/mL; 100 µL/well; PerkinElmer Inc., USA) and allowed to attach overnight before removing the medium and washing twice with 1× HBSS (pH 7.4), after which different concentrations of nanocarrier suspensions (1-2000 µg/mL) were added into the wells (1× HBSS, pH 7.4, 100 µL/well). Positive and negative controls of Triton X-100 and 1× HBSS (pH 7.4), respectively, were used. After 24 h incubation, the wells were washed once with 1× HBSS (pH 7.4) and the number of viable cells was assayed with CellTiter-Glo (Promega® Corporation, USA). The luminescence was measured on a Varioskan Flash Fluorometer (Thermo Fisher Scientific, USA). All the experiments were performed at least in triplicate.

### 2.11. Cell proliferation tests

The *in vitro* proliferation effect of multi-drug loaded PSi@AcDX-CPP was evaluated in MCF-7 and MDA-MB-231 cells. The cells were seeded in 96-well plates and processed as described above. After washing, the cells were treated with serial concentrations of bare MTX, PTX and SFN combinations (0.01−100 µg/mL for each drug) or corresponding drug-loaded PSi@AcDX-CPP (1× HBSS, pH 7.4; 100 µL).

Owing to the poor solubility of both PTX and SFN, P-188 was added into the 1× HBSS (pH=7.4), showing no significant impact on cell proliferation. After 24 h incubation, the wells were washed once with 1× HBSS (pH 7.4) and the number of viable cells was assayed with CellTiter-Glo (Promega® Corporation, USA). The luminescence was measured on a Varioskan Flash fluoromete. All the experiments were performed at least in triplicate.

## 3. Results and Discussion

### 3.1. Fabrication and characterization of the nanocomposites

The development of the previously described microfluidic technology and the precise regulation of the fluids' flow rates made possible to control the nanoparticles size [29], resulting in the fabrication of homogenously dispersed multi-drug loaded pH-responsive nanocomposites. The fabrication process has been already shown in **Figure 1**. Due to its properties, and despite its negative ζ-potential, AcDX was chosen as polymer for encapsulating bare PSi. Since the cell surface is also negatively charged, AcDX would likely hinder cell uptake of the particles, creating therefore the need to functionalize the surface of PSi@AcDX with aminooxyacetyl-K-$(R)_9$-COOH, a positively charged CPP.

The TEM images, dynamic light scattering (DLS) for size, and ζ-potential for charge measurements, and FTIR spectra allowed the characterization of the prepared nanocarriers, as exposed in **Figure 2.**

TEM images of the surface of PSi (**Figure 2**a), AcDX (**Figure 2**b), PSi@AcDX (**Figure 2**c), and PSi@AcDX-CPP (**Figure 2**d) demonstrated the successful encapsulation of PSi within the AcDX particles. In comparison to the irregularly shaped PSi, the resulting nanocomposites reveal spherical structure and improved surface smoothness. Furthermore, it is displayed that CPP functionalization of PSi@AcDX did not interfere with their morphology.

Moreover, by using less magnification in TEM, it is possible to appreciate an overall view of the particles (**Figure 2**e), confirming the homogeneous dispersed size of PSi@AcDX-CPP. The comparison of the size distribution of the particles was obtained using the Zetasizer instrument (**Figure 2**f), which determined that the average particle size for PSi@AcDX-CPP was bigger than the bare PSi particles (~ 350 nm versus ~180 nm), but similar to AcDX and PSi@AcDX. Theoretically, if the particles were to pursue in vivo testing, these dimensions of PSi@AcDX-CPP would allow them to passively accumulate in the tumor sites. The accumulation mechanism relies on a passive diffusion or convection across the leaky and hyperpermeable tumor vasculature, as well as on the absence of an effective lymphatic drainage system in the tumor microenvironment. This phenomenon is referred to as the enhanced permeation and retention (EPR) effect. [42]

Additionally, in order to confirm the encapsulation of PSi nanoparticles, ζ-potential measurements and FTIR analyses were carried out on the samples. As it can be seen (**Figure 2**g), there are oscillations in ζ-potential values of the several particles, at each step of the process. Firstly, the ζ-potential for PSi was positive due to the amine termination that

resulted from PSi's surface functionalization with APTES (*ca.* 32.4±0.7 mV), while after its encapsulation within AcDX the resulting particle presented a ζ-potential similar to AcDX (*ca.* -46.3±2.9 mV), suggesting a successful encapsulation. After the functionalization with CPP, the final ζ-potential of PSi@AcDX-CPP turned into positive (*ca.* 48.3±3.0 mV), as expected.

In the ATR–FTIR spectra (**Figure 2**h), the spectrum for PSi@AcDX is identical to the one for AcDX, which, in addition to the disappearing peak in PSi spectrum (circled in red), indicates the proper encapsulation of PSi within AcDX. Moreover, in comparison with PSi@AcDX, the presence of the amide I (ν(C=O), 1657 cm-1) and II (δ(N–H), 1537 cm-1) bands (circled in green) presented after functionalization with CPP assured the proper conjugation of PSi@AcDX with aminooxyacetyl-K-$(R)_9$-COOH.

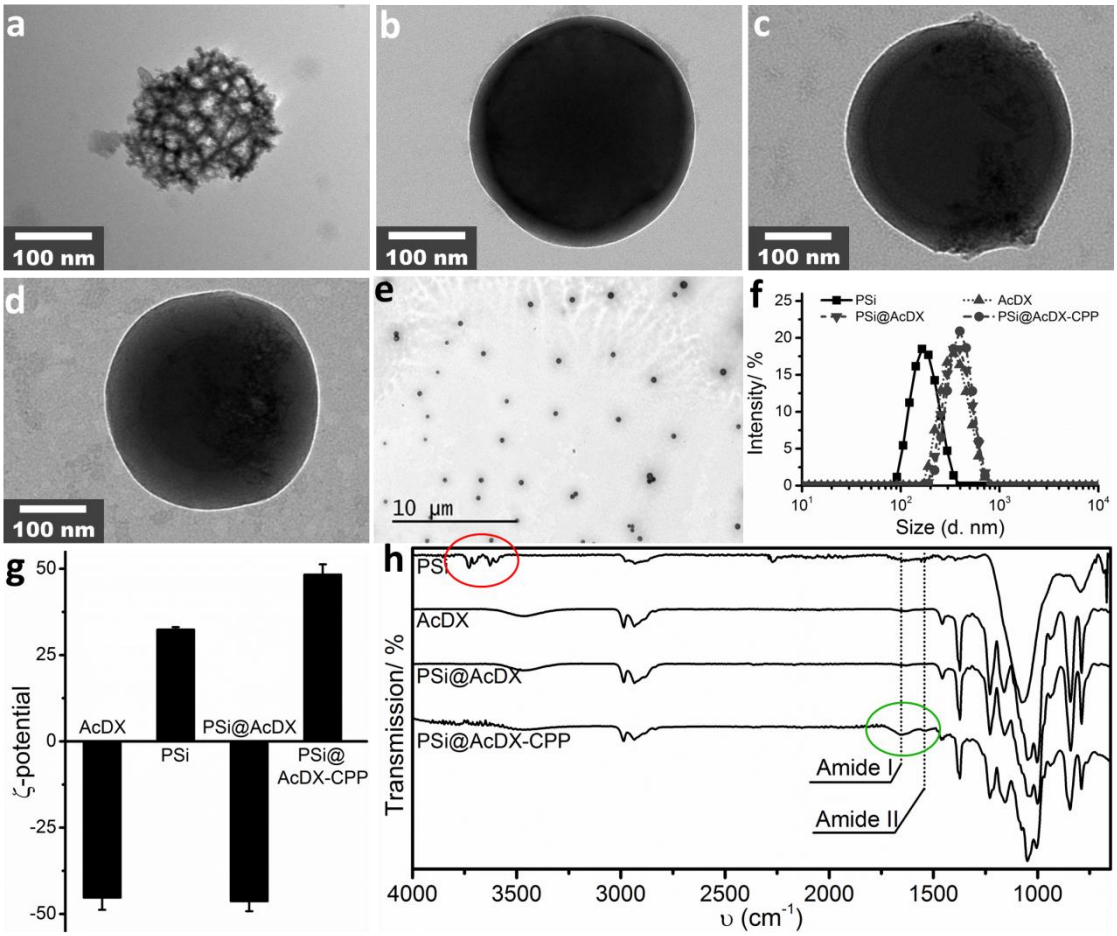


**Figure 2.** *Characterization of the fabricated nanocarriers. TEM images of PSi (a), AcDX (b), PSi@AcDX (c), and PSi@AcDX-CPP (d), as well as an overall image of PSi@AcDX-CPP taken with less magnification (e). Intensity based (f) comparison of size distributions of the different particles. The ζ-potential (g) measurements of the different samples, during the assembly process, reassured the successful encapsulation and production of*

*PSi@AcDX-CPP. ATR-FTIR spectra (h) of the samples were used to unravel chemical moieties for monitoring the fabrication of CPP-functionalized PSi@AcDX.*

### 3.2. Dissolution profile of the nanocomposites

AcDX polymer was prepared by reversibly modifying dextran with acetal-protecting groups, which, as discussed elsewhere,[34] has granted it acidic pH-responsive behavior,[34] ideal for protecting the loaded drug payloads of MTX, PTX, and SFN from unwanted release at physiological pH 7.4. After the cellular uptake of the nanocarriers, AcDX is supposed to degrade inside the acidic endosomal enviroment, releasing the encapsulated cargo as the pH value decreases to pH 5.0.

Therefore, in order to demonstrate how the dissolution behavior of AcDX at different pH-values affected the structure and integrity of the prepared nanocomposites, the samples underwent dissolution tests followed by TEM imaging.

AcDX and PSi@AcDX-CPP were put into different buffer solutions, simulating the extracellular and intracellular conditions (pH 7.4 and pH 5.0, respectively) for 6h, during which samples were collected and analyzed at different time-points.

A thorough examination of the digital photos obtained in accordance with the TEM imaging (**Figure 3**a and b), led to the conclusion that both AcDX (**Figure 3**a) and PSi@AcDX-CPP (**Figure 3**b) maintained the structural integrity at pH 7.4. When tested in mild acidic condition, bare AcDX became smaller with the passage of time, eventually disappearing. Similarly, at pH 5.0, PSi@AcDX-CPP nanocomposites were dissolved, and the exposure of the encapsulated PSi, at 0.5h, culminated with the complete release of the PSi nanoparticles after the degradation of the polymeric matrix.

These dissolution phenomenons were clearly visible by simple macroscopic observation of the samples (**Figure 3**c), as it is possible to observe that the nanocarriers incubated at pH 7.4 remained as an opaque suspension throughout the 6.0 hours, except for PSi, which aggregated due to the presence of buffer salts. In contrast, the suspensions of AcDX, and PSi@AcDX-CPP, at pH 5.0, became completely transparent at the end-point, hence suggesting the complete hydrolysis and full degradation of the polymeric layer, with the consequent disaggregation of the tested nanocarriers.

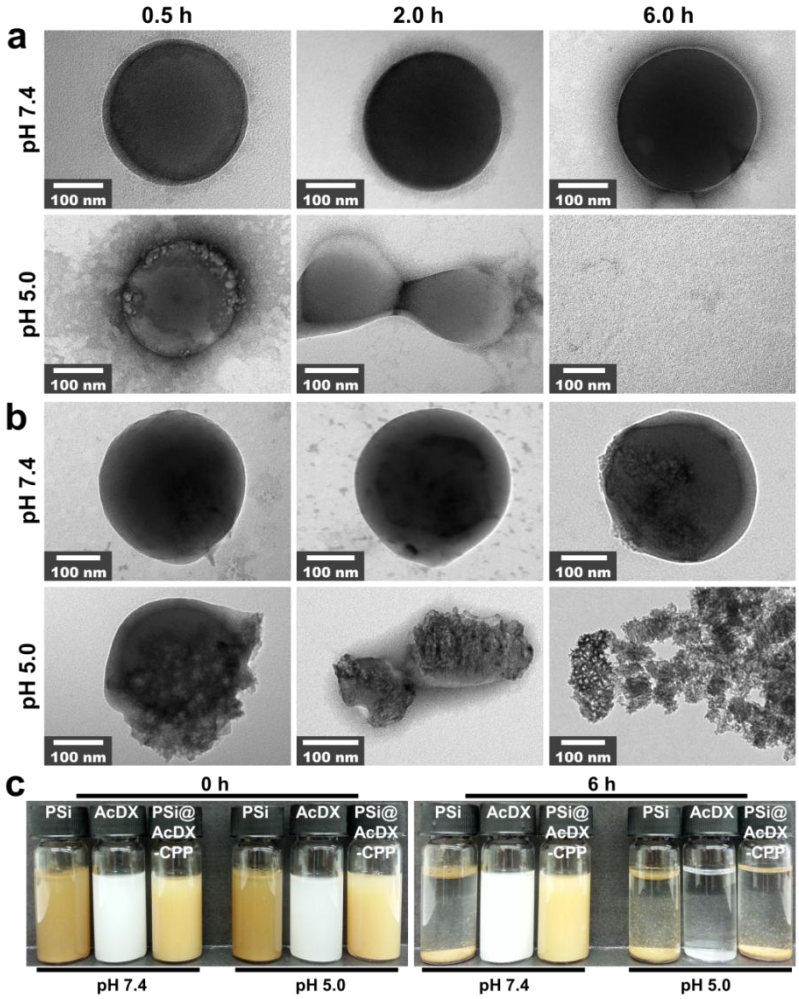


**Figure 3.** *Dissolution behavior of the nanocomposites at diferent pH conditions as a function of time. TEM images of AcDX (a) and PSi@AcDX-CPP (b) under extracellular and intracellular conditions (pH 7.4 and pH 5.0, respectively) for 0.5, 2.0, and 6 h. Time lapse photos of PSi, AcDX, and PSi@AcDX-CPP under extracellular and intracellular conditions, at the 6 h time-point (c).*

These results indicate that the assembled nanocarriers were able to successfully bare extracellular environment without significant damages to its structure or variations in its content. As shown, PSi@AcDX-CPP is likely to remain stable until it reaches the aimed pH-value for decomposition and consequent release of their multi-drug loaded content – the intracellular location.

### 3.3. Drug loading and *in vitro* drug release profile of PSi@AcDX-CPP

As previously stated, AcDX pH-responsive polymer is responsible for protecting the encapsulated drugs and drug-loaded PSi, preventing their degradation and consequent early

release in the blood. This way, the multi-drug loaded nanocomposites would desirable maintain its stability and structure until the release of their payload after cellular uptake.

Owing to the different and complex physical properties of the drugs and constituents involved, precise and ratiometric controlled multi-drug loading is the key step in the preparation of the presented DDS.

As discussed elsewhere,[22] the release rate of a loaded drug was found to depend on the characteristic dissolution behavior of the drug substance. In this regard, further studies have shown the importance of PSi for improving the physicochemical properties of poorly soluble drug molecules, enhancing their dissolution/release profiles as it allows the drugs to retain their non-crystalline (amorphous) form.[17, 22] On the other hand, however, when the dissolution rate of the bare drug was high, its encapsulation within the PSi's interconnected empty pores caused a delayed release of the drug in test [22] (theoretically, these findings would apply to the highly soluble drug MTX).

Based in these findings, and owing to MTX, PTX, and SFN different solubility behaviors, PSi plays a crucial role in the triple-loading of PSi@AcDX-CPP, by storing and protecting the highly soluble MTX from fast release. Due to their high solubility in ethanol, but poor solubility in aqueous phase, the loading degree of PTX and SFN could be easily tailored by changing the drug concentration in the inner fluid (it was tailored to *ca.* 5% (ww)). Contrarily, MTX is very hydrophilic, which, as it can be seen in **Figure 4**, results in a 0.14% loading degree, when dispersed only in ethanol/AcDX (**Figure 4**a). However, by first loading the MTX into the PSi particles and then disperse them in the inner fluid, the degree of MTX loaded into the newly assembled PSi@AcDX was significantly enhanced to *ca.* 4% (w/w) (**Figure 4**a), proving the importance of PSi in optimizing the loading of incompatible drugs in the same carrier.

Regarding the encapsulation yield (**Figure 4**b), and having as reference the quantity of drug in solution, high amounts of PTX and SFN were successfully encapsulated into the particles, being important to refer the increase in the encapsulation degree of MTX in the presence of PSi, which illustrates the storage capacity of these compounds. The CPP-functionalization did interfere neither with the drug loading degree nor with the encapsulation degree of the particles.

*In vitro* simulations at both steady and changing pH-values allowed the evaluation of the drug release profile of PSi@AcDX-CPP at different time-points, for 24 h. In order to keep the SINK conditions for all the payloads (especially for the PTX, and SFN), P-188 was added into the release media.

By simulating extracellular and intracellular conditions, it was shown that the nanocomposites present close to zero release of the loaded PTX (**Figure 4**c), SFN (Figure 4d), and MTX (**Figure 4**e) at pH 7.4, but rapid and constant release in the presence of conditions resembling the endosomal environment.

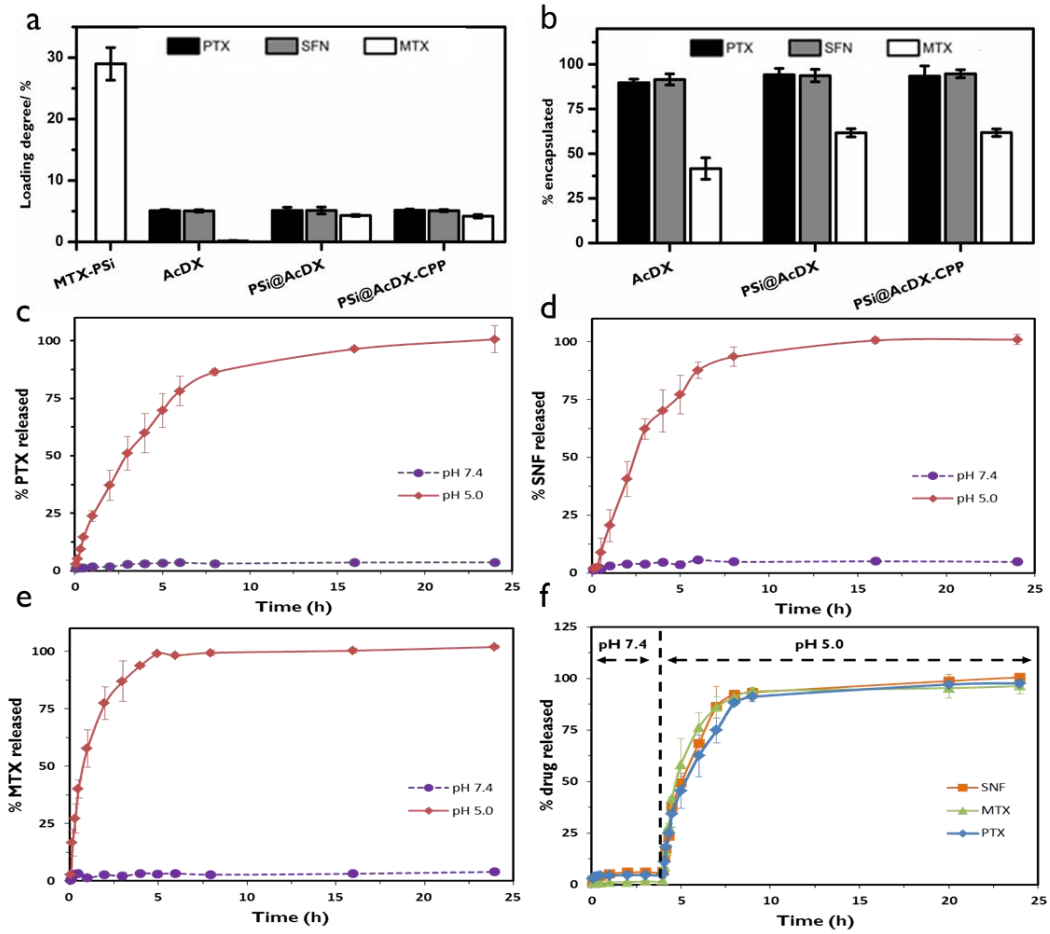


**Figure 4.** *Loading and release of payloads from the PSi@AcDX-CPP. The loading degree (a) and encapsulation efficiency (b) of PTX, SFN, and MTX were calculated based on the total weight of the drug-loaded samples. The loading degree and encapsulation efficiency of the drug-loaded PSi@AcDX-CPP were all compared with those of AcDX. The release profiles of PTX (c), SFN (d), and MTX (e) from the PSI@AcDX-CPP were obtained at pH 7.4, and 5.0, at 37 °C. The release profiles of the payloads from the nanocomposites were also tested with continuous changes in the pH-values starting from pH 7.4 to 5.0 (f). Data represent mean ± s.d. (n = 3).*

With the aim of measuring the total released drugs, the nanocomposites were also tested with continuous changes in the pH-values, starting from pH 7.4 to 5.0 (**Figure 4**f). As expected, at first there was only a marginal amount of drug released, but once the pH-value

dropped to 5.0, it was shown that almost all the amount of the loaded drugs was released within 24 h.

These significant pH-dependent drug release profiles suggest that all the three drugs were strongly trapped inside the PSi@AcDX-CPP, responding to a specific pH-stimulus for releasing the payloads, in a polymer degradation dependent manner.

This way, PSi@AcDX-CPP has suggested to behave as a successful pH-response nanocarrier. Its proven stability at pH 7.4, resulting in minimal drug release, advocates a reliable systemic safety profile of the carriers which, overtime, could help overcoming the high toxicity levels associated with cancer therapy.

### 3.4. Cellular uptake analysis of the fabricated particles

The CPP used to functionalize the presented drug delivery system has been proved successful for intracellular delivery of a range of different molecules, from peptides to nanoparticles.[37] Hence, and resorting to the fluorescence properties of FITC; PSi, PSi@AcDX, and PSi@AcDX-CPP samples (100 μg/mL) were labelled in order to oversee the extent of their cellular association with MCF-7, and MDA-MB-231 cancer cells, after 6h incubation. After this incubation period and posterior washing, cells were harvested and treated with trypan blue to quench the fluorescence of possible surface adherent particles, thus discriminating the cell-particle association and particle internalization in order to prevent possible mistakes in excess.

The flow cytometry device is an important tool for quantifying the number of cells that have internalized the labelled particles. Through the analysis of the results, it is possible to establish a direct relationship between the fluorescence intensity and the number of cells that have incorporated the particles.

In **Figure 5**, MCF-7, and MDA-MB-231(**Figure 5**a, b, respectively) cell counts obtained from flow cytometry measurements are shown. Each curve represents the fluorescence of 10.000 cells, after being treated with the different tested particles. Cells that hadn't been in contact with any particles were used as control (grey fill).

In both **Figure 5**a and **Figure 5**b the flow cytometry histograms show an increase in the cellular associated fluorescence for PSi, and PSi@AcDX-CPP curves, while the PSi@AcDX treated cells revealed similar fluorescence to the one read for the control. As Figure 6c corroborates, there is a significant cellular association for PSi, and PSi@AcDX-CPP particles, as seen from the increase of mean fluorescence intensity of the cells. The mean fluorescence intensity is considerably higher for PSi@AcDX-CPP, indicating greater cellular internalization, most likely due to the presence of CPP.

The lack of cellular association of PSi@AcDX might result not only from the AcDX's negative surface charge, but as well from its chemical moieties, which can act as a steric barrier against non-specific protein adsorption.[43]

Considering the control as baseline (its fluorescent values are considered as zero), **Figure 6**d, through comparison, allows the quantitative analysis of the fluorescent cells. Hence, it is shown that, overtime, PSi@AcDX-CPP have been internalized by more than 80% of the available cells, in each cell line, showing improved cellular affinity when compared to PSi (<32%)

These results are important to assess the role of the CPP functionalization in the cellular uptake of our nanocomposites. Due to the presence of CPP, the PSi@AcDX-CPP system has shown to be successfully uptaken by the cells. These positive cellular responses to the particles encourage their further development for future therapeutic applications.

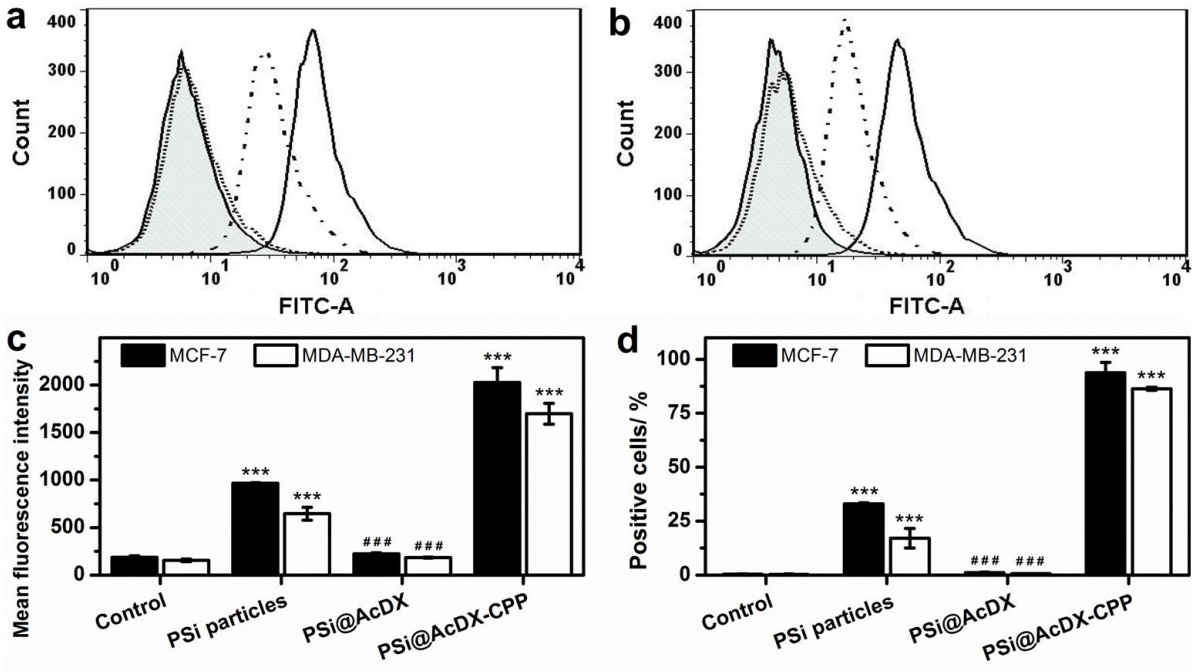


**Figure 5.** *Flow cytometry histograms of MCF-7 (a), and MDA-MB-231 (b) show the fluorescence intensity of control cells (gray fill), cells incubated with PSi particles (dash-dot line), PSi@AcDX (short dot line), and PSi@AcDX-CPP (solid line). The resulting mean fluorescence intensity (c) gives a qualitative perspective of the cellular association, but it is through the comparison of the fluorescence values of the different samples with the control that is possible to draw a baseline that allows the posterior calculation of the percentage of positive cells (d) after interaction with each nanocarrier. The mean fluorescence intensity and percentage of positive cells are compared with the control cells (*); PSi@AcDX-CPP were compared with those of PSi@AcDX (#).Data represent mean ± s.d. (n = 3).*

### 3.5. Cellular tests: cell viability and proliferation

TEM characterization, followed by dissolution and release experiments for testing the physical properties of PSi@AcDX-CPP, represents an important mean for analyzing the particles behavior, and assessing their possible potential as a future therapeutic DDS.

After those initial procedures, it is of the greatest importance to understand how these particles would react within the human body, once they reach the cellular interface: how the bare particles would interfere with the cellular viability and in what way the drugs loaded inside would affect the proliferation rate of the selected cancer cells.

For these purposes, we have conducted the cellular tests in two different breast cancer cells, MCF-7 and MDA-MB-231.

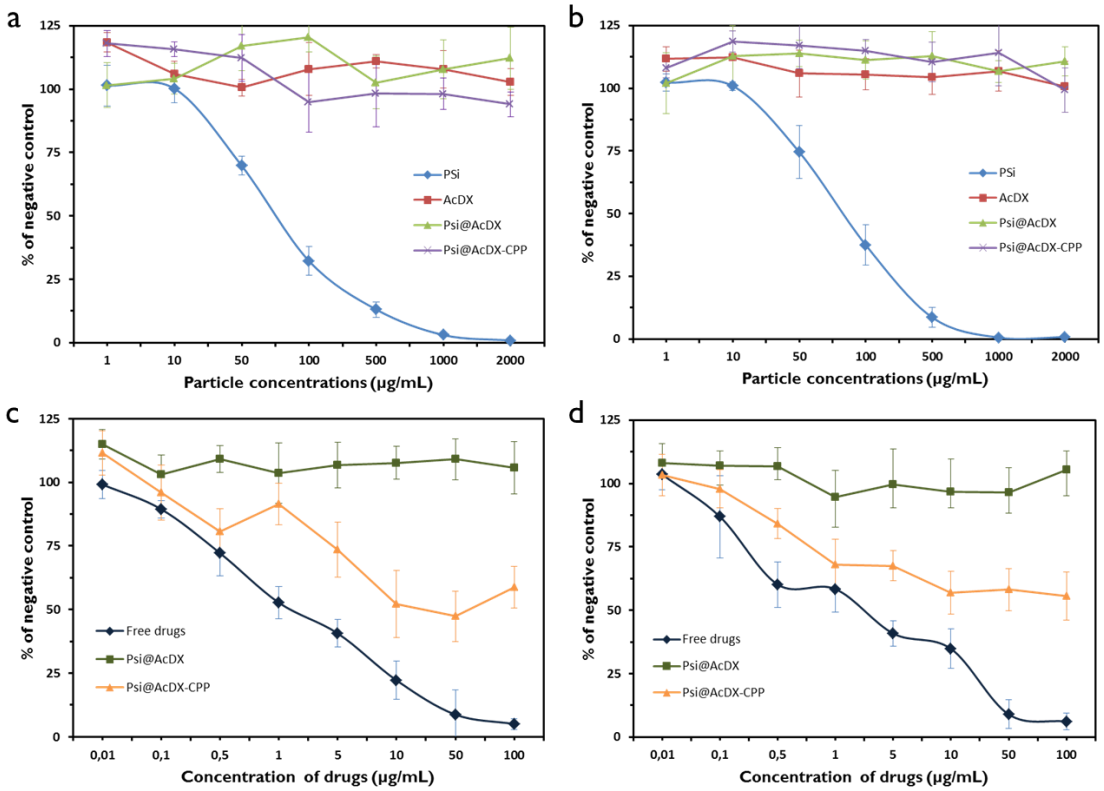


**Figure 6**. *Interactions with breast cancer cells assessed by ATP-based luminescence assay. Cytocompatibility of PSi, AcDX, PSi@AcDX, and PSi@AcDX-CPP, at different concentrations, with MCF-7 (a) and MDA-MB-231 (b) cells after 24h incubation at pH 7.4. The 1×HBSS (pH 7.4) served as negative control. Proliferation profiles of MCF-7 (c) and MDA-MB-231 (d) cells treated with serial concentrations of multiple-drug loaded nanocomposites for 24h, at pH 7.4. The concentrations of PTX, SFN, and MTX (1:1:1, w/w/w) ranged from 0.01 to 100 µg/mL for each drug, being the combination of free PTX, SFN, and MTX selected as negative control. All experiments were conducted at 37 °C. Data represent mean ± s.d. (n = 3).*

In order to compare the cytocompatibility of the PSi encapsulated nanocomposites with bare PSi, a range of particle concentrations between 1 and 2000 μg/mL was chosen and PSi, AcDX, PSi@AcDX, and PSi@AcDX-CPP were tested in both MCF-7 and MDA-MB-231 cultures, using 1× HBSS (pH 7.4) as negative control.

As shown in **Figure 6**a and **Figure 6**b (MFC-7 and MDA-MB-231 respectively), all the samples demonstrate minimum levels of cytotoxicity at low concentrations but, from 10 μg/mL forward, PSi revealed to be extremely hazardous, killing almost all the cells as the concentration increases and reaches 1000 μg/mL. On the other hand, PSi encapsulated particles have evenly revealed a cytocompatibility close to 100% throughout the assortment of concentrations.

Even though highest concentrations of PSi@AcDX-CPP caused a slight decrease in cellular viability (possibly caused by cellular uptake of the particle, due to CPP, with consequent pH-responsive polymer degradation and exposure of PSi), the results obtained from this experiment are clear. Encapsulating PSi within a biocompatible matrix significantly improves its cytocompatibility, allowing it to be harmlessly used as part of DDS. Furthermore, it is shown that PSi encapsulated compounds present no concentration-related toxicity for the cells, being able to be administrated at high dosages, if necessary.

Regarding the proliferation tests, proliferation profiles of MCF-7 (**Figure 5**c) and MDA-MB-231 (**Figure 5**d) were obtained by comparing the proliferation indices of cells that had previously been treated with serial concentrations of multiple-drug loaded nanocomposites, with the ones from cells treated with a combination of free PTX, SFN, and MTX (negative control). Both experiments occurred at pH 7.4 and, as before, in the presence of P-188, for increasing the solubility of PTX and SFN in aqueous medium. P-188 showed no significant impact on MCF-7, and MDA-MB-231 cell proliferation.

As expected, the combination of free PTX, SFN, and MTX clearly reduced the cell growth in a concentration dependent manner (**Figure 5**c-d). Further analysis of both those figures shows that drug-loaded PSi@AcDX had no meaningful effect in cell proliferation, suggesting the inexistence of drug release, possibly due to the lack of cellular uptake of the particle.

Oppositely, it is possible to notice a decrease in cellular proliferation caused by PSi@AcDX-CPP. As the concentrations of the loaded drugs increase, the effect of PSi@AcDX-CPP in the cellular proliferation rates can almost be compared to the effect of the free drugs. However, the existing difference between them can be attributed to the fact that only part of the drug-loaded PSi@AcDX-CPP particles was uptaken by the cells and, consequently, was able to dissolve and release the loaded drugs *in situ*.

Overtime, as the drug concentration reaches 100 μg/mL, it was shown that PSi@AcDX-CPP caused an impressive 50% decrease in the proliferation rate of cancer cells. These results suggest an effective cellular internalization of PSi@AcDX-CPP, promoted by the CPP, which allowed the particles to degrade and release their drug payload, in the presence of intracellular environment.

## 4. Conclusion

Herein, we report a valid formulation for a multicomponent PSi-based DDS for breast cancer therapy.

The referred system has ultimately proved to provide sustained, ratiometric and pH-controlled release of multiple drugs. The initial one-step microfluidic nanoprecipitation resulted in tunable and precise encapsulation of PTX, SFN, and MTX within the biocompatible PSi and the pH-responsive AcDX polymer, followed by particles' functionalization with a cellular uptake enhancer – CPP.

Taking leverage of PSi's structure, large surface area, great pore volume, and profiting from AcDX sealing role and microfluidics tunable and accurate focusing processes, it was possible to alleviate the formulation problems caused by the unique physico-chemical properties inherent to the different drugs. The end result – PSi@AcDX-CPP - was a multidrug-loaded nanoparticle with encapsulated PTX, SFN, and MTX, otherwise incompatible in a single nanocarrier.

As justified throughout the present monograph, PSi@AcDX-CPP has met the established objectives, demonstrating reproducible fabrication process, homogenously dispersed size, pH-responsive dissolution behavior, sustained overtime drug release, particle cytocompatability and inhibition of cellular proliferation, due to its effective cellular internalization and consequent release of the multi-drug content.

Owing to their high cytocompatibility and the absence of concentration-related toxicity, it is possible to administrate high dosages of PSi@AcDX-CPP, feasibly with different drug loaded ratios and concentrations, according to the desired therapeutic indication.

The impact of multi–drug loaded nanocomposites on cell proliferation demonstrated to be highly in accordance with their cell uptake potential, promoted by CCP. However, due to its lack of target selectivity, CPP's unique "trojan horse" approach could lead to serious safety and toxicity concerns to normal tissues or organs for *in vivo* application.[37]

For these reasons, and even thought PSi@AcDX-CPP figures as a promising prototype drug carrier for breast cancer therapy, there is the need for further research in

order to incorporate various stimuli-responsive mechanisms for targeted and controllable CPP-based drug delivery, hence increasing particles' systemic safety.

## 5. References


1. Farokhzad, O.C. and R. Langer, *Impact of nanotechnology on drug delivery.* ACS Nano, 2009. **3**(1): p. 16-20.
2. Ferrari, M., *Nanovector therapeutics.* Curr Opin Chem Biol, 2005. **9**(4): p. 343-6.
3. Cyrus, T., G.M. Lanza, and S.A. Wickline, *Molecular imaging by cardiovascular MR.* J Cardiovasc Magn Reson, 2007. **9**(6): p. 827-43.
4. West, J.L. and N.J. Halas, *Applications of nanotechnology to biotechnology commentary.* Curr Opin Biotechnol, 2000. **11**(2): p. 215-7.
5. Vaseashta, A. and D. Dimova-Malinovska, *Nanostructured and nanoscale devices, sensors and detectors.* Science and Technology of Advanced Materials, 2005. **6**(3-4): p. 312-318.
6. *The Project on Emerging Nanotechnologies, The Woodrow International Center for Scholars.* http://www.nanotechproject.org/, 2008.
7. Shahani, S., *Advanced Drug Delivery Systems: New Developments, New Technologies. BBC Research.* http://www.bccresearch.com/report/PHM006G.html (Accessed 23 December 2010). 2009.
8. Santos, H.A., et al., *Multifunctional porous silicon for therapeutic drug delivery and imaging.* Curr Drug Discov Technol, 2011. **8**(3): p. 228-49.
9. Wang, Y., et al., *Co-Delivery of Drugs and DNA from Cationic Core-Shell Nanoparticles Self-Assembled from a Biodegradable Copolymer.* Nature Materials, 2006. **5**(10): p. 791-796.
10. Zhang, H.B., G.J. Wang, and H.A. Yang, *Drug Delivery Systems for Differential Release in Combination Therapy.* Expert Opinion on Drug Delivery, 2011. **8**(2): p. 171-190.
11. Kratz, F. and A. Warnecke, *Finding the Optimal Balance: Challenges of Improving Conventional Cancer Chemotherapy Using Suitable Combinations with Nano-Sized Drug Delivery Systems.* Journal of Controlled Release, 2012. **164**(2): p. 221-235.
12. Liu, Q., et al., *Delivering Hydrophilic and Hydrophobic Chemotherapeutics Simultaneously by Magnetic Mesoporous Silica Nanoparticles to Inhibit Cancer Cells.* International Journal of Nanomedicine, 2012. **7**: p. 999-1013.
13. Kolishetti, N., et al., *Engineering of Self-Assembled Nanoparticle Platform for Precisely Controlled Combination Drug Therapy.* Proceedings of the National Academy of Sciences of the United States of America, 2010. **107**(42): p. 17939-17944.
14. Deshayes, S., et al., *Delivery of Proteins and Nucleic Acids Using a Non-covalent Peptide-Based Strategy.* Advanced Drug Delivery Reviews, 2008. **60**(4-5): p. 537-547.
15. Canham, L.T., et al., *Derivatized mesoporous silicon with dramatically improved stability in simulated human blood plasma.* Advanced Materials, 1999. **11**(18): p. 1505-+.
16. Liu, D.F., et al., *Microfluidic Templated Mesoporous Silicon-Solid Lipid Microcomposites for Sustained Drug Delivery.* Acs Applied Materials & Interfaces, 2013. **5**(22): p. 12127-12134.
17. Santos, H.A., J. Salonen, and L.M. Bimbo, *Porous Silicon for Drug Delivery*, in *Encyclopedia of Metalloproteins*, R.H. Kretsinger, V.N. Uversky, and E.A. Permyakov, Editors. 2013, Springer: New York. p. 1773-1781.
18. Stewart, M.P. and J.M. Buriak, *Chemical and biological applications of porous silicon technology.* Advanced Materials, 2000. **12**(12): p. 859-869.
19. Canham, L.T., *Bioactive silicon structure fabrication through nanoetching techniques.* Advanced Materials, 1995. **7**(12): p. 1033-&.
20. Salonen, J., V.P. Lehto, and E. Laine, *The room temperature oxidation of porous silicon.* Applied Surface Science, 1997. **120**(3-4): p. 191-198.
21. Salonen, J., et al., *Stabilization of porous silicon surface by thermal decomposition of acetylene.* Applied Surface Science, 2004. **225**(1-4): p. 389-394.
22. Salonen, J., et al., *Mesoporous silicon microparticles for oral drug delivery: Loading and release of five model drugs.* Journal of Controlled Release, 2005. **108**(2-3): p. 362-374.

23. Limnell, T., et al., *Surface chemistry and pore size affect carrier properties of mesoporous silicon microparticles.* International Journal of Pharmaceutics, 2007. **343**(1-2): p. 141-147.
24. Ganan-Calvo, A.M., et al., *Building functional materials for health care and pharmacy from microfluidic principles and Flow Focusing.* Advanced Drug Delivery Reviews, 2013. **65**(11-12): p. 1447-1469.
25. Capretto, L., et al., *Microfluidic and lab-on-a-chip preparation routes for organic nanoparticles and vesicular systems for nanomedicine applications.* Advanced Drug Delivery Reviews, 2013. **65**(11-12): p. 1496-1532.
26. Nguyen, N.T., et al., *Design, fabrication and characterization of drug delivery systems based on lab-on-a-chip technology.* Advanced Drug Delivery Reviews, 2013. **65**(11-12): p. 1403-1419.
27. Valencia, P.M., et al., *Microfluidic technologies for accelerating the clinical translation of nanoparticles.* Nature Nanotechnology, 2012. **7**(10): p. 623-629.
28. Hashimoto, M., R. Tong, and D.S. Kohane, *Microdevices for Nanomedicine.* Molecular Pharmaceutics, 2013. **10**(6): p. 2127-2144.
29. Kim, Y.T., et al., *Mass Production and Size Control of Lipid-Polymer Hybrid Nanoparticles through Controlled Microvortices.* Nano Letters, 2012. **12**(7): p. 3587-3591.
30. Kim, Y., et al., *Single step reconstitution of multifunctional high-density lipoprotein-derived nanomaterials using microfluidics.* ACS Nano, 2013. **7**(11): p. 9975-83.
31. Tsui, J.H., et al., *Microfluidics-assisted in vitro drug screening and carrier production.* Advanced Drug Delivery Reviews, 2013. **65**(11-12): p. 1575-1588.
32. Vladisavljevic, G.T., et al., *Industrial lab-on-a-chip: design, applications and scale-up for drug discovery and delivery.* Adv Drug Deliv Rev, 2013. **65**(11-12): p. 1626-63.
33. Makila, E., et al., *Amine Modification of Thermally Carbonized Porous Silicon with Silane Coupling Chemistry.* Langmuir, 2012. **28**(39): p. 14045-14054.
34. Bachelder, E.M., et al., *Acetal-derivatized dextran: An acid-responsive biodegradable material for therapeutic applications.* Journal of the American Chemical Society, 2008. **130**(32): p. 10494-+.
35. Cohen, J.A., et al., *Acetal-modified dextran microparticles with controlled degradation kinetics and surface functionality for gene delivery in phagocytic and non-phagocytic cells.* Adv Mater, 2010. **22**(32): p. 3593-7.
36. Cui, L., et al., *Mannosylated dextran nanoparticles: a pH-sensitive system engineered for immunomodulation through mannose targeting.* Bioconjug Chem, 2011. **22**(5): p. 949-57.
37. Huang, Y., et al., *Curb challenges of the "Trojan Horse" approach: smart strategies in achieving effective yet safe cell-penetrating peptide-based drug delivery.* Adv Drug Deliv Rev, 2013. **65**(10): p. 1299-315.
38. Beaudette, T.T., et al., *Chemoselective Ligation in the Functionalization of Polysaccharide-Based Particles.* Journal of the American Chemical Society, 2009. **131**(30): p. 10360-+.
39. Chu, L.Y., et al., *Monodisperse thermoresponsive microgels with tunable volume-phase transition kinetics.* Advanced Functional Materials, 2007. **17**(17): p. 3499-3504.
40. Bimbo, L.M., et al., *Functional hydrophobin-coating of thermally hydrocarbonized porous silicon microparticles.* Biomaterials, 2011. **32**(34): p. 9089-9099.
41. Liu, D.F., et al., *Nanostructured Porous Silicon-Solid Lipid Nanocomposite: Towards Enhanced Cytocompatibility and Stability, Reduced Cellular Association, and Prolonged Drug Release.* Advanced Functional Materials, 2013. **23**(15): p. 1893-1902.
42. Maeda, H., *The enhanced permeability and retention (EPR) effect in tumor vasculature: The key role of tumor-selective macromolecular drug targeting.* Advances in Enzyme Regulation, Vol 41, 2001. **41**: p. 189-207.
43. Park, J.Y., et al., *Cell-repellant Dextran Coatings of Porous Titania Using Mussel Adhesion Chemistry.* Macromolecular Bioscience, 2013. **13**(11): p. 1511-1519.